

# UV Curable Robust Durable Hydrophobic Coating Based on Epoxy Polyhedral Oligomeric Silsesquioxanes (EP-POSS) and Their Derivatives

Peng Zhang,\* Ban Qin, and Jianhui Xia\*

Cite This: *ACS Omega* 2022, 7, 17108–17118

Read Online

ACCESS |



Metrics &amp; More

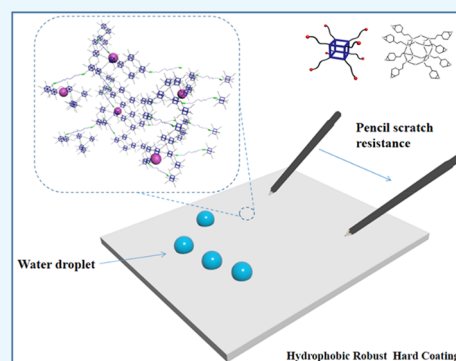


Article Recommendations



Supporting Information

**ABSTRACT:** Hydrophobic coatings have considerable potential applications in many fields. Ease of operation and high durability are essential for practical use. Fast curing and being solvent-free are a plus, and if they possess certain characteristics (antigraffiti, good adhesion, high hardness, heat resistance, wide range of applicability, etc.) at the same time, it is a dream solution. Herein, a facile one-step approach with the above features was reported for a UV curable robust hydrophobic coating based on Epoxy Polyhedral Oligomeric Silsesquioxanes (EP-POSSs). The structure and surface morphology of these EP-POSSs and their derivatives were systematically studied. Because of the core-in-cage structure which was constructed by repeating units of  $R-Si(O_{1/2})_3$  and the strong covalent bonds of Si–C and Si–O, the coatings displayed high pencil hardness (6–8H), high thermal stability with initial decomposition temperature around 350–400 °C, and a high water contact angle (up to 108.06°) even after outdoor exposure for a month. These POSSs and their derivatives are expected to find uses in various applications such as stain resistance, self-cleaning, scratch resistance, and cigarette moxibustion resistance of wood furniture, kitchenware, and medical and industrial appliances.



## 1. INTRODUCTION

Hydrophobic materials can prevent moisture and dust for electronic components, prevent drug pollution or residue for medical devices, prevent pollution and self-cleaning for surface coatings, etc. Due to the tremendous potential of water-repellent applications in different fields, hydrophobic materials have attained intensive attention.<sup>1,2</sup> Hydrophobicity is represented by water contact angle. In materials science, surface tension and Gibbs free energy are different expressions of physical parameters of the same value and the same dimension. The contact angle is the tangent of the drop profile at the triple point (three-phase contact point) where the liquid–gas interface meets the solid–liquid interface, and it provides an inverse measure of wettability. The hydrophobicity of a solid surface is mainly determined by Gibbs free energy of the solid surface when the chemical composition of the liquid and gas phases is fixed. And the Gibbs free energy of a solid surface mainly depends on inherent properties of solid materials and their surface microstructures. Therefore, it can be simply considered that hydrophobicity mainly depends on the inherent characteristics of the material and molding process.

The “lotus effect” theory<sup>3</sup> was put forward by Barthlott and Neinhuis in 1997. Inspired by the “lotus effect”, scientists found that a surface structure constructed by hierarchical micro-nanostructures can greatly reduce the area of the solid–liquid interface and surface tension, which improves the surface

hydrophobicity of solid materials.<sup>4,5</sup> There are many methods to construct hierarchical micro-nanostructures,<sup>6</sup> such as physical or chemical deposition,<sup>7</sup> electrochemical methods, electrospinning, etc. Currently, most hydrophobic coating materials are fabricated through imitated plant or animal hierarchical micro-nanostructures<sup>8–13</sup> or created artificial hierarchical micro-nanostructure surfaces via multistep procedures.<sup>14–22</sup> The hierarchical micro-nanostructure is easily destroyed by slight external forces due to insufficient strength. Thus, it is difficult to achieve the expected purpose of durable hydrophobicity.<sup>23,24</sup> Therefore, it is urgent to find a material with low surface Gibbs free energy and high mechanochemical strength. The common strategy is inducing self-healing groups into a formula system to maintain its hierarchical micro-nanostructure as much as possible<sup>25,26</sup> or building a microstructure to improve its mechanochemical strength.<sup>27,28</sup> However, these methods may induce poor overall performance due to dispersion problems, body strength, and so on. Therefore, it is necessary to seek answers in the field of low surface Gibbs free energy materials; there are several ways to

Received: January 26, 2022

Accepted: April 13, 2022

Published: May 13, 2022



induce long-chain alkyl and fluoroalkyl groups into the polymers or particle fillers and modify them at the molecular level.<sup>29,30</sup>

Considering Gibbs free energy and mechanochemical strength, organic coating materials are suitable for preparing hydrophobic coatings, for instance silicone, polyurethane, epoxy, acrylate, etc. However, it is difficult for traditional organic coating materials to adapt to the increasingly stringent environmental protection emission regulations and the requirements of high-turnover production lines as a result of using organic solvents, slow curing, high energy consumption during the curing process, or poor thermal stability above 150–200 °C. The differences between traditional commercial hydrophobic coatings and this work (UV cured) were shown in Table 1. Polyhedral Oligomeric Silsesquioxanes (POSSs), a

**Table 1. Comparison between This Work and Traditional Commercial Coatings**

item	traditional commercial hydrophobic coatings			this work (UV cured)
	moisture cured	heat cured	UV cured <sup>a</sup>	
pencil hardness (H)	2–6	2–6	3–4	>7–8
cure time	several days	several hours	few seconds	few seconds
decomposition (°C)	250–350 °C	250–350 °C	300–350 °C	350–400 °C
adhesion				
PET	2–5	1–4	5, or fail	0–1
ABS, PC	1–4	0–3	2–3	0–1
metal	1–3	0–3	5, or fail	1–2
glass	2–5	2–4	5, or fail	1–2

<sup>a</sup>The formula of the UV cured coating can be seen in formula b of Table S2 in the Supporting Information.

type of intramolecular organic–inorganic hybrid material with low surface Gibbs energy and excellent mechanochemical strength,<sup>31,32</sup> are suitable for preparing nanolevel hybrid materials.<sup>33</sup> In addition, one of the advantages is that POSSs can be designed for UV curing, which could greatly expand its application value. According to previous literature,<sup>34–37</sup> Epoxy Polyhedral Oligomeric Silsesquioxanes (EP-POSSs), in Figure 1 below, show an excellent mechanochemical improvement effect on coating materials.

In this work, we built a robust, durable hydrophobic coating with functional EP-POSSs and their derivatives containing long-chain alkyl groups and/or fluoroalkyl groups, functionalized surface-modified nanoparticles, cation photoinitiators, and suitable organic solvents as building blocks. These series of

functional EP-POSSs and their derivatives were synthesized by a sol–gel method through hydrolysis and a polycondensation process of specified silanes with epoxy groups, nanoparticles prepared by several methods, the first was from the mixture of tetraethyl orthosilicate (TEOS) and specific epoxysilane through core–shell copolymerization by sol–gel method; the second was modifying the surface of micro- or nanofillers with specific silane or other treatment agents. The selected fillers included fumed silica, colloidal silica, etc. As illustrated in Figure 2, the robust durable hydrophobic coating, which is based on EP-POSSs, derivatives, micro- or nanofillers, cationic photoinitiators, and other substances, was selected through experimental design, formulated into a liquid, coated on PET, and completely cured, and other processes studied the relationship among hydrophobicity, hardness, strength, abrasion resistance, etc.

The series of UV-curable coatings based on EP-POSSs are described in this article. The advantages are being solvent-free; being completely cured in a few seconds; having good adhesion on varieties of substrates, such as glass, wood, plastic, and metal; and having high pencil hardness and considerable scratch resistance, temperature resistance, and excellent aging properties, etc. The series of POSSs and their derivatives have a wide range of application prospects in industrial coatings.

## 2. EXPERIMENTAL SECTION

Ikada<sup>38</sup> commented that there were two methods for surface modification: one was the graft coupling method; the other was the graft polymerization method. There were three ways of creating silica-based nanofillers in this paper. The first was surface modified solid nanoparticles<sup>39</sup> (fumed silica, AEROSIL 200) via functional silane; the second was nanoparticles generated by core–shell copolymerization from colloidal silica (Grace LUDOX AM) and functional silane;<sup>40–42</sup> the third was nanoparticles and/or their graft copolymers generated by the sol–gel process of tetraethyl orthosilicate<sup>43</sup> (TEOS) and functional silane.<sup>44</sup> Six basic polymers (303-POSS, 3F-303-polymer, C8-303-polymer, 402-polymer, 3F-402-polymer, and C8-402-polymer) were synthesized through a sol–gel method, and the derivative (amino-PDMS)-(303-POSS) polymer was synthesized by an epoxy ring-opening reaction with amino groups. The three kinds of nanofillers (3F-SiO<sub>2</sub>, 3F-AM, and C8-AM; 10%-303-TEOS and 30%-303-TEOS; and 50%-303-TEOS) were separately prepared by different surface treatment processes.

The coating formula consisted of the above compounds mixed in preset proportions, cured by cationic photoinitiators for subsequent tests.

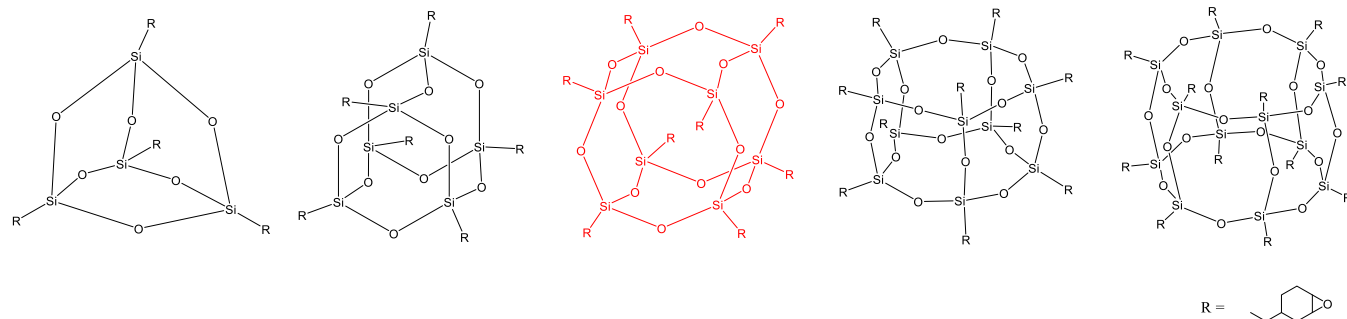


**Figure 1.** POSSs of cages with different numbers and represented by T8R8 marked red.

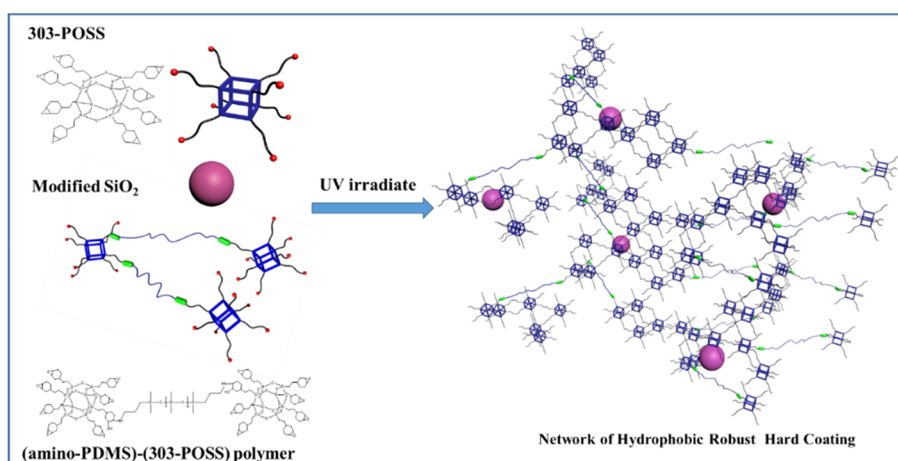


Figure 2. Chemical reaction involved in this robust hydrophobic coating.

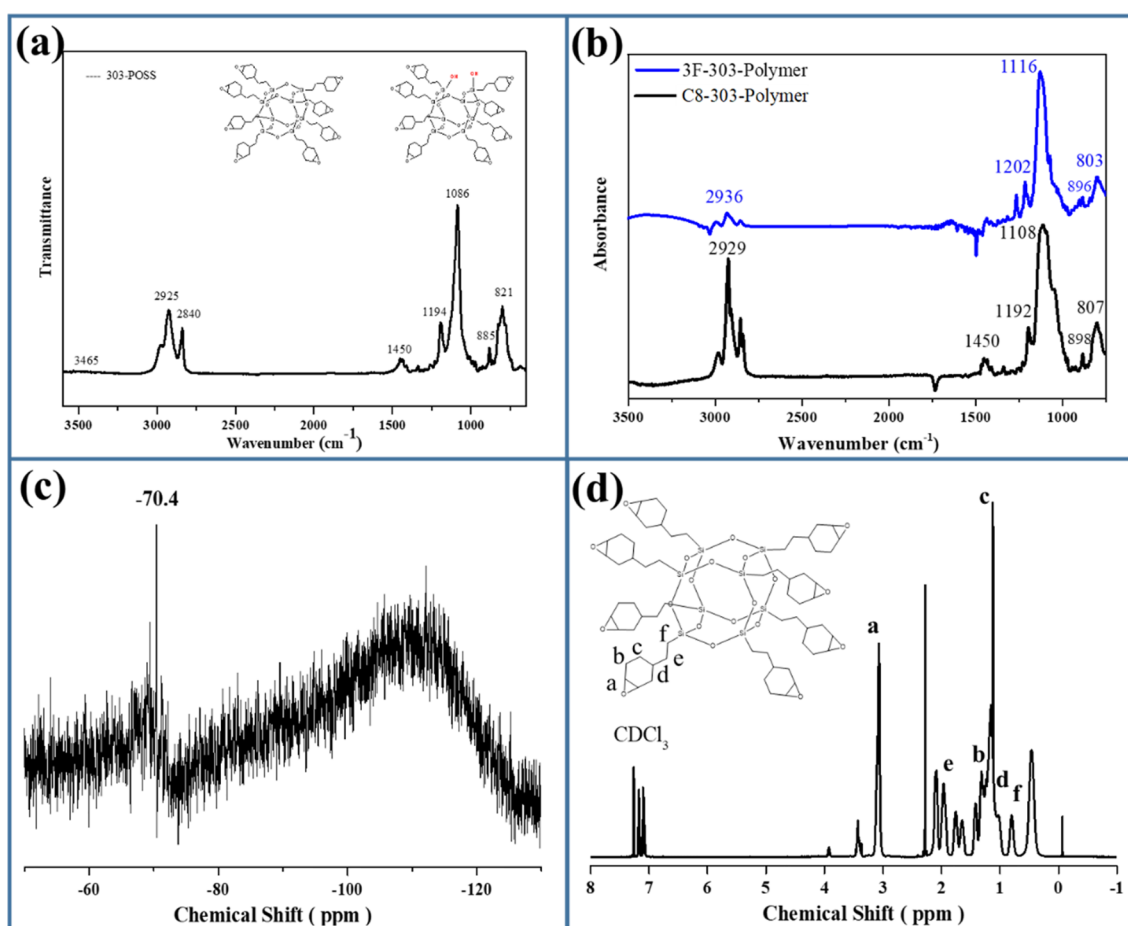


Figure 3. ATR-FTIR, <sup>1</sup>H NMR, and Si NMR of 303-POSS and their derivatives. (a) The ATR-FTIR spectrum of 303-POSS. (b) The ATR-FTIR spectrum of 3F-303-Polymer (blue) and C8-303-Polymer (black). (c) The Si NMR spectrum of 303-POSS. (d) The <sup>1</sup>H NMR spectrum of 303-POSS.

Detailed experimental processes, characterizations, and other experimental procedures are presented in the section S1 of the Supporting Information.

### 3. RESULTS AND DISCUSSION

A series of UV curable organosilicon polymers (303-POSS, 3F-303-polymer, C8-303-polymer, 402-polymer, 3F-402-polymer, and C8-402-polymer) were synthesized by a sol–gel method;

it is believed that these polymers were POSSs and/or their derivatives from the results of GPC, IR, <sup>1</sup>H NMR, and Si NMR characterizations. The polymers were subsequently used without further purification.

303-POSS, 3F-303-polymer, and C8-303-polymer had a high pencil hardness for high cross-linking density but lacked flexibility which is caused by the rigidity of the core-in-cage structure and high cross-linking density. So, a series of

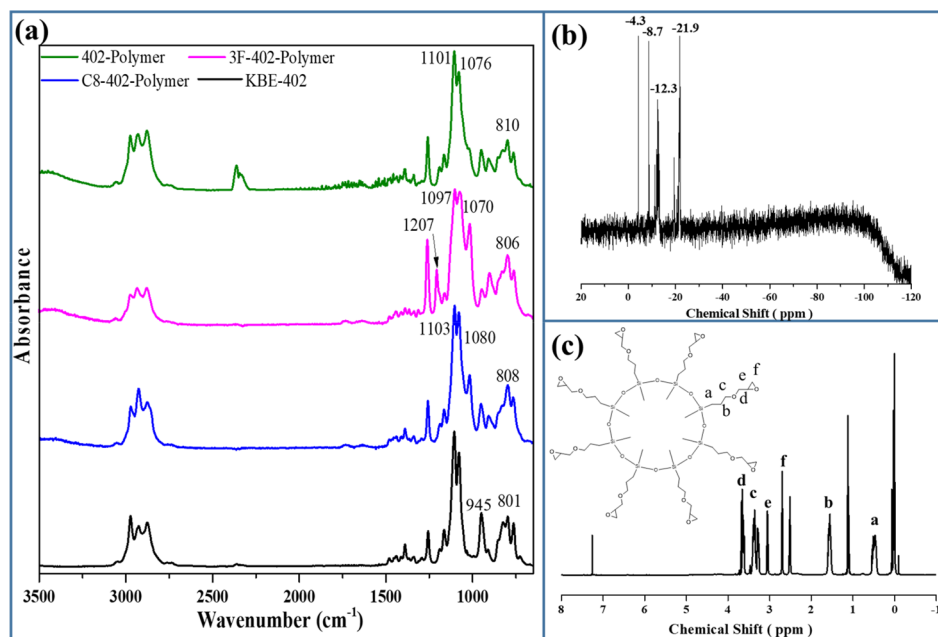


**Figure 4.** ATR-FTIR, <sup>1</sup>H NMR, and Si NMR of 402-polymer and its derivatives. (a) The ATR-FTIR spectrum of KBE-402 silane, 402-polymer, 3F-402-polymer, C8-402-polymer. (b) The Si NMR spectrum of 402-polymer. (c) The <sup>1</sup>H NMR spectrum of 402-polymer.

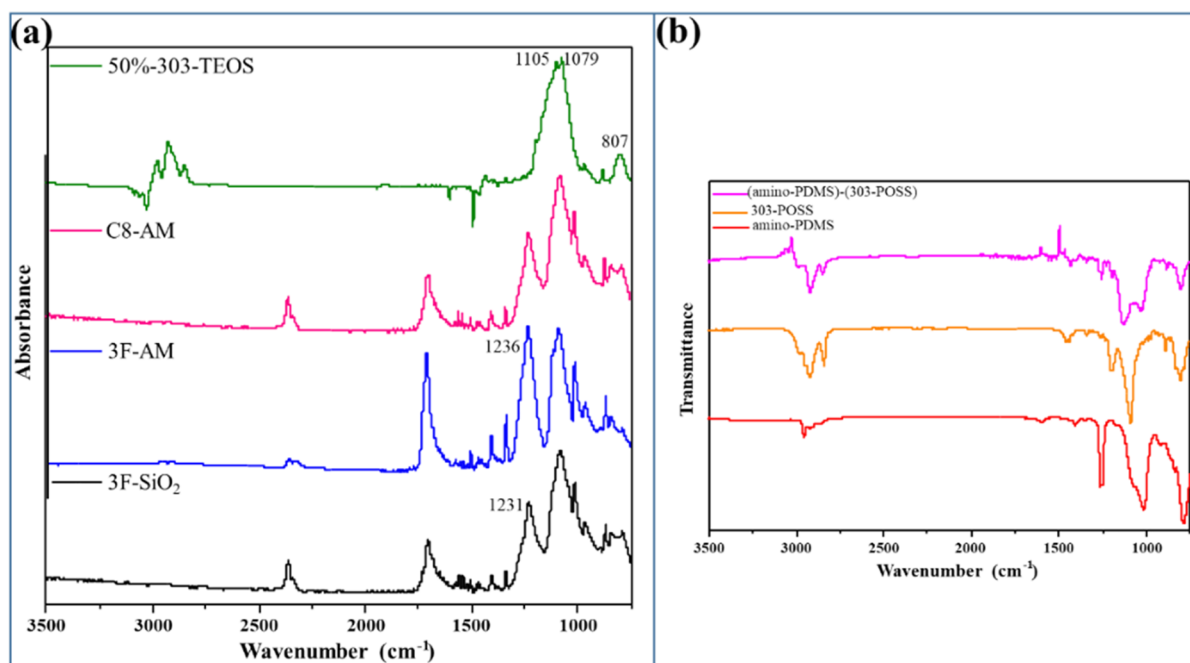


**Figure 5.** ATR-FTIR of nanoparticles and (amino-PDMS)-(303-POSS) polymer. (a) The ATR-FTIR spectrum of 50%-303-TEOS polymer, C8-AM, 3F-AM, and 3F-SiO<sub>2</sub>. (b) The ATR-FTIR spectrum of 303-POSS, amino-PDMS, and the (amino-PDMS)-(303-POSS) polymer.

polymers with the same or similar epoxy functional groups and several chain segments was prepared; they were 402-polymer, 3F-402-polymer, C8-402-polymer, and (amino-PDMS)-(303-POSS) polymer, as described in the experimental section, Supporting Information section S1. As expected, they all had flexible chain segments and functional groups dispersed. In addition, to balance the relationship between flexibility and hardness, a series of surface-modified nanofillers was prepared.

In this paper, an easy-to-operate, fast curing, and environmentally friendly UV curable coating was prepared. With properties of good adhesion (0–2 grade, X-cut, cross-cut) on

plastics, glass, metal, and other substrates; high hardness (pencil hardness of 6–8H); excellent hydrophobic properties (contact angle of 108.06°); durability; and good heat resistance (the initial decomposition temperature was up to 350–400 °C), it is believed that the UV curable robust hydrophobic coating based on EP-POSSs described in this article is better than the traditional commercial UV curable coating.

**3.1. Structure Characterization of Experimental Samples.** The ATR-FTIR and Si NMR spectra of 303-POSS and the ATR-FTIR of 3F-303-Polymer and C8-303-

Polymer are shown in Figure 3. As shown in Figure 3a, the peaks at 821  $\text{cm}^{-1}$ , 885  $\text{cm}^{-1}$ , 1086  $\text{cm}^{-1}$ , 1450  $\text{cm}^{-1}$ , and 2925  $\text{cm}^{-1}$  are the Si–C stretching vibration, epoxy group stretching vibration, Si–O–Si stretching vibration, C–O stretching vibration, and C–H stretching vibration, respectively. The cage-like Si–O–Si opposition stretching vibration is observed at 1194  $\text{cm}^{-1}$ . In addition, the wavenumber ranging from 3200 to 3500  $\text{cm}^{-1}$  disappeared, which represents an alcoholic hydroxyl group stretching vibration, indicating that the KBM-303 was consumed completely. The ATR-FTIR spectrum of 3F-303-Polymer (blue) and C8-303-Polymer (black) are shown in Figure 3(b). The peaks at 896 and 898  $\text{cm}^{-1}$  are the epoxy group; those at 1202  $\text{cm}^{-1}$  and 2800–3000  $\text{cm}^{-1}$  are C–F and (–CH<sub>2</sub>–) stretching vibrations, respectively. In Figure 3c, the chemical shift showed a sharp peak at –70.4 ppm indicating the main target product was a core-in-cage structure. And the chemical structure of 303-POSS was also confirmed by the <sup>1</sup>H NMR spectrum (CDCl<sub>3</sub>):  $\delta$  (ppm) 0.35–0.56 (s, 2H, –Si–CH<sub>2</sub>–), 0.95–1.07 (s, 1H, –CH<sub>2</sub>–CH–CH<sub>2</sub>–), 1.87–2.05 (m, 2H, –CH<sub>2</sub>–CH<sub>2</sub>–CH–), 1.08–1.22 (m, 2H, –CH<sub>2</sub>–CH<sub>2</sub>–CH<sub>2</sub>–), 1.86–2.16 (m, 2H, –CH–CH<sub>2</sub>–CH<sub>2</sub>–), 3.01–3.16 (s, 1H, –O–CH<sub>2</sub>–CH<sub>2</sub>–), 7.25 (s, CDCl<sub>3</sub>), the spectra of which can be seen in Figure 3d.

The ATR-FTIR spectra of 402-Polymer (green), 3F-402-Polymer (pink), C8-402-Polymer (blue), and KBE-402 silane (black) are shown in Figure 4a. And the peaks at 945  $\text{cm}^{-1}$ , 1207  $\text{cm}^{-1}$ , and 2800–3000  $\text{cm}^{-1}$  are the epoxy group and C–F and –CH<sub>2</sub>– stretching vibrations, respectively. In Figure 4b, the Si NMR spectrum of 402-Polymer exhibits several sharp peaks at chemical shift peaks of –4.3, –8.7, –12.3, and –21.9 ppm, indicating that the Si element possessed several chemical environments. The <sup>1</sup>H NMR spectrum of 402-Polymer (CDCl<sub>3</sub>):  $\delta$  (ppm) 0.36–0.6 (m, 2H, –Si–CH<sub>2</sub>–), 1.45–1.72 (m, 2H, –CH<sub>2</sub>–CH<sub>2</sub>–CH<sub>2</sub>–), 2.42–2.58 (s, 2H, –O–CH<sub>2</sub>–CH<sub>2</sub>–), 3.0–3.08 (s, 1H, –CH<sub>2</sub>–CH<sub>2</sub>–O), 3.18–3.31 (m, 2H, –CH<sub>2</sub>–CH<sub>2</sub>–O–), 3.54–3.73 (m, 2H, –O–CH<sub>2</sub>–CH–O–), which are shown in Figure 4c. According to the the Si NMR and <sup>1</sup>H NMR spectra, 402-Polymer was a composite that consisted of different lengths of siloxane chain segments.

The chemical structure of surface-modified nanoparticles and the (amino-PDMS)-(303-POSS) polymer were also measured by ATR-FTIR. The ATR-FTIR spectrum of 50%-303-TEOS (green), C8-AM (pink), 3F-AM (blue), and 3F-SiO<sub>2</sub> (black) is seen in Figure 5a. The peaks around 1231 and 807  $\text{cm}^{-1}$  are attributed by C–F group vibration and C–O–C group vibration, respectively.

The ATR-FTIR spectra of the (amino-PDMS)-(303-POSS) polymer (pink), 303-POSS (orange), and amino-PDMS (red) are shown in Figure 5b. In the ATR-FTIR spectrum of amino-PDMS, the peaks around 2800–2900  $\text{cm}^{-1}$  are attributed to –NH<sub>2</sub> group vibration; the peak of –NH<sub>2</sub> group vibration disappeared in the ATR-FTIR spectrum of the (amino-PDMS)-(303-POSS) polymer for the –NH<sub>2</sub> in amino-PDMS reacted with the epoxy groups in 303-POSS.

**3.2. The Differences of Parameters of Synthetic Polymers.** The data of GPC, IR, <sup>1</sup>H NMR, and Si NMR showed that the 303-POSS may be a T8R8 or T10R10 core-in-cage structure. Since the standard bond angle<sup>45</sup> of O–Si–O of T8H8 is 108°18' and T8V18 is 110°48', which are close to the standard bond angle of tetra-substituted silicon of 109°28', trisilanol intermediates tend to form a T8R8 structure in the polycondensation process. However, the IR spectrum showed an obvious peak of the silica hydroxyl group around 3400

$\text{cm}^{-1}$ . The NMR spectrum showed large deviations, and the GPC data showed that the molecular weight of 303-POSS was 1472 (molecular weight of standard structure T8R8 is 1418.20, T10R10 is 1772.75). The deviations of GPC, IR, and NMR data were first attributed to the difference between the synthesized product and standard structure; the synthesized product was a mixture of similar structures not separated and purified by column chromatography. Second, they were attributed to measurement error and the accuracy of the instrument.

The polycondensation process of 402-polymer was similar. It tends to form a polymer with a long-chain and/or cyclic structure in the polycondensation process because disilanol intermediates can only polymerize by a chain-growth mechanism. So, 402-polymer is a compound with 12 siloxane chains, in theory, according to the molecular weight of 2443. The length of the chain depends on many factors, such as temperature, time, and the pH value of the system of polycondensation processes etc. The PDI of 402-polymer (PDI = 1.284) was significantly higher than 303-POSS (PDI = 1.014) for less selectivity of disilanol intermediates and high cage-forming selectivity of trisilanol intermediates.

The molecular weight and PDI of 50%-303-TEOS ( $M_n$  = 3028,  $M_w$  = 4208, PDI = 1.390) polymer were significantly higher than those of 303-POSS ( $M_n$  = 1472,  $M_w$  = 1493, PDI = 1.014). Because 50%-303-TEOS is a homogeneous polycondensation process of trisilanol intermediates, the polycondensation of trisilanol intermediates was affected by tetrasilanol intermediates and underwent random core–shell copolymerization with tetra-silanol intermediates in the 50%-303-TEOS polymer polycondensation process.

**3.3. The Balance among Hardness, Hydrophobicity, Durability, and Flexibility.** The surface-modified fumed silica (3F-SiO<sub>2</sub>), modified nanoparticles (3F-AM and C8-AM), and the 50%-303-TEOS polymer have good compatibility with 303-POSS for the same –Si–O– chain segment and nanoscale size. A coating formula with the same equivalent of fillers, meaning the same number of moles of Si(O<sub>1/2</sub>)<sub>4</sub>, was considered as equivalent silica, and it did not matter if it was from fumed silica AEROSIL 200, Grace LUDOX AM, or tetraethyl orthosilicate. Compared with three kinds of nanofillers, 3F-SiO<sub>2</sub> had the largest thickening effect and poorest reinforcing effect, followed by 3F-AM, and 50%-303-TEOS polymer had the best effect. 50%-303-TEOS is commendable for its high fill ratio; for example, even the dosage was 50%. The percentage of Si(O<sub>1/2</sub>)<sub>4</sub> (equivalent silica) in the coating formula system was 12.6%. The formula system was still fluid. A formula system with the other two fillers at this ratio showed extremely high viscosity. It seems that the 50%-303-TEOS polymer constructed by an intramolecular hybrid structure had better compatibility with the coating formula system and can play a better role than 3F-SiO<sub>2</sub>, 3F-AM, and C8-AM.

The high cross-linking density of 303-POSS leads to a too high hardness, ease of cracking, etc. The importance of 402-Polymer, 3F-402 polymer, and the (amino-PDMS)-(303-POSS) polymer comes into play at this time. Due to a long-chain or ring structure with a UV curable group at each siloxane chain segment, 402-polymer and the 3F-402 polymer have excellent flexibility and less cross-linking density. The structure of the (amino-PDMS)-(303-POSS) polymer is amazing because the middle part is flexible siloxane chain

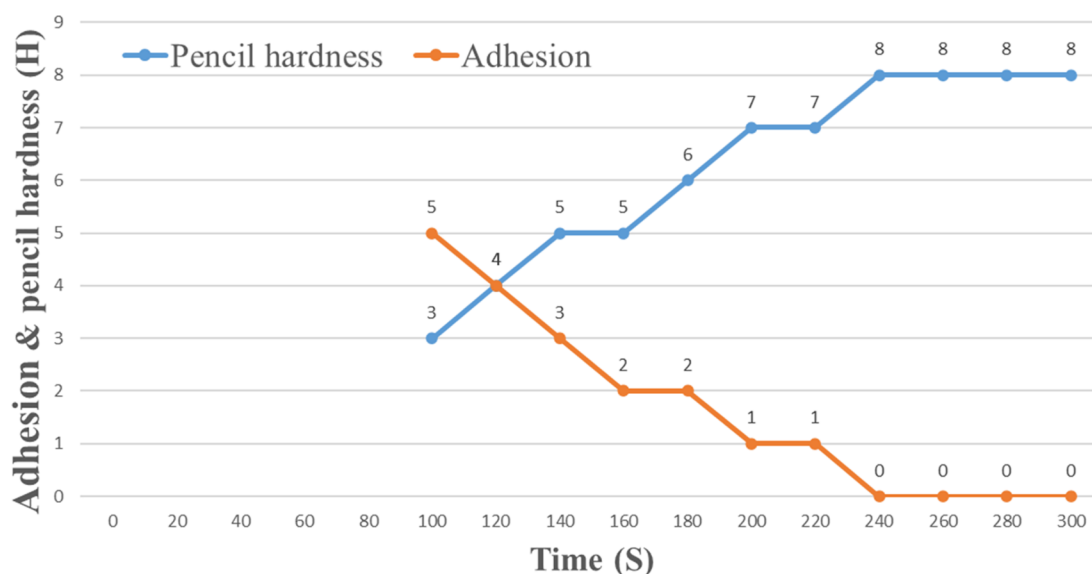


Figure 6. Effect of UV irradiation time to pencil hardness and adhesion properties.

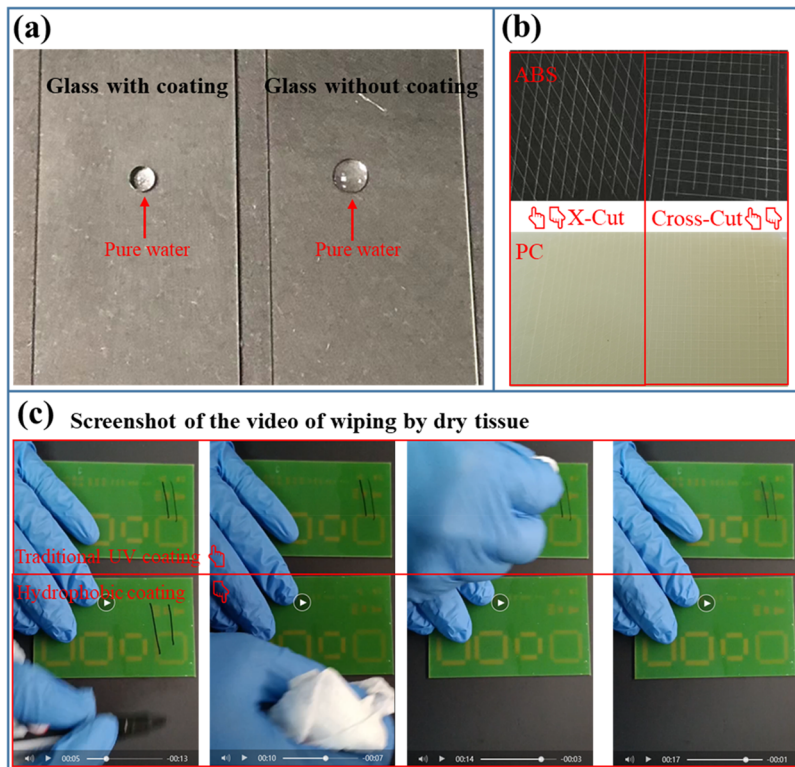


Figure 7. Apparent properties of hydrophobic coatings. (a) Image of glasses coated by a durable hydrophobic hard coating (left) and without coating (right). (b) Images of PC and ABS coated by a durable hydrophobic coating, and then cut into cross-cut (up) and X-cut (down). (c) Image of wiping ink stains by dry tissue.

segments of customized length and seven reactive groups gathered at both ends of the chain.

By adjusting the proportions of the materials above, we obtained a coating with both central cross-linking and certain flexible linking, which significantly improved the flexibility of the coating without greatly reducing the hardness and strength.

303-POSS has excellent adhesion on varieties of substrates and an approximately 6–8H pencil hardness and contact angle of  $88.70^\circ$ . 303-POSS and derivatives can be cured in a few seconds. Figure 6 shows the relationship between the

properties and curing time of the hydrophobic coatings described in this paper. The hardness and adhesion increase with the curing process, until completely cured.

**3.4. Adhesion of the Series of Robust Durable Hydrophobic Coatings.** Figure 7a shows the image of glass coated with a robust hydrophobic coating (left) and without coating (right). It can be seen that glass coated with the coating showed better hydrophobic ability than that without coating. In addition, the adhesion was investigated via cross-cut and X-cut on the surface of polycarbonate (PC) and

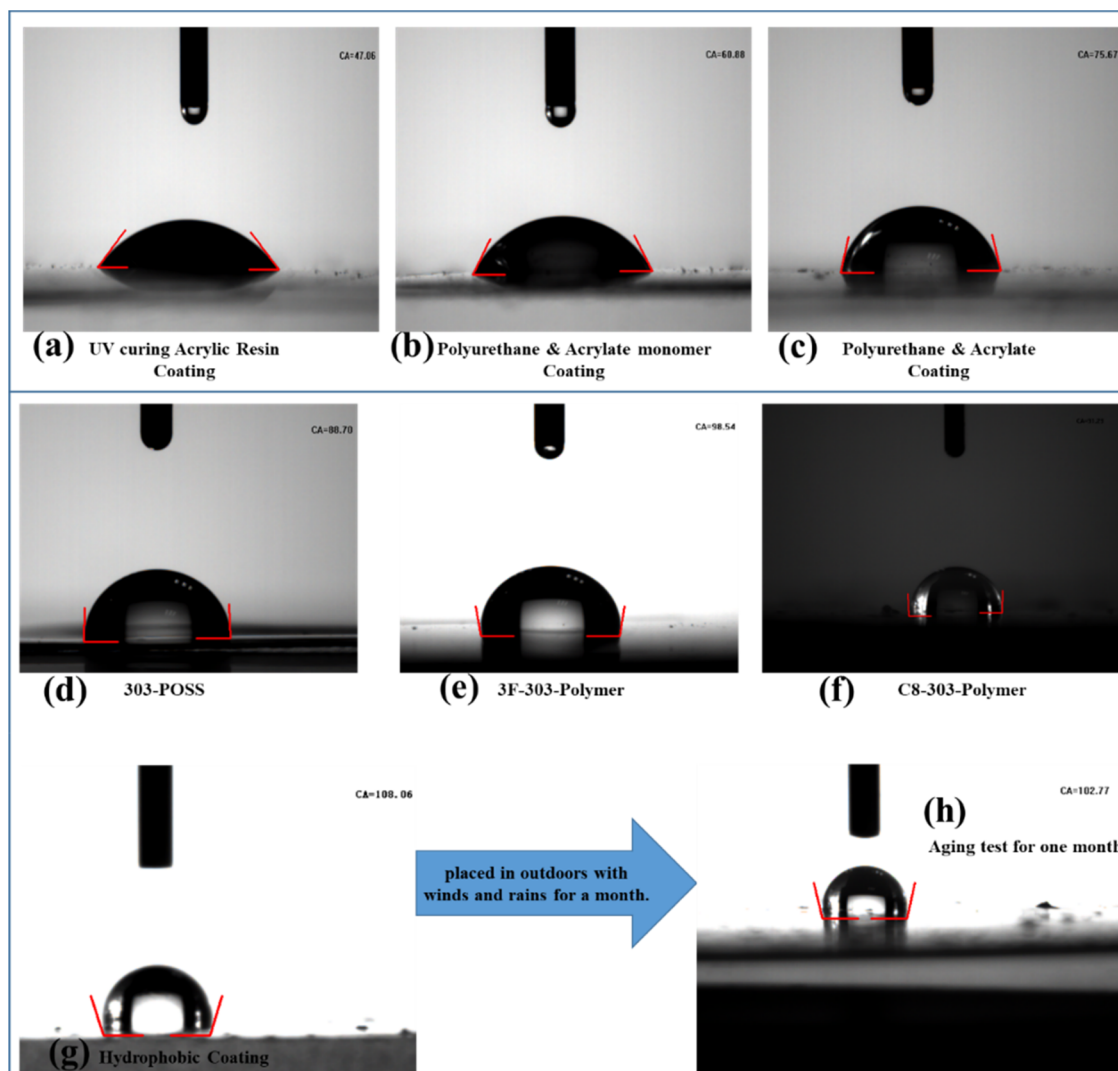


**Figure 8.** Contact angles of different coatings. (a) Image of the contact angle ( $47.06^\circ$ ) of the traditional UV coating based on acrylate resin. (b) Image of the contact angle ( $60.88^\circ$ ) of the traditional UV coating based on a mixture of 2f PUA and EA. (c) Image of the contact angle ( $75.67^\circ$ ) of the traditional UV coating based on 6f and 9f PUA. (d) Image of the contact angle ( $88.70^\circ$ ) of the UV coating based on 303-POSS. (e) Image of the contact angle ( $98.54^\circ$ ) of the UV coating based on 3F-303-polymer. (f) Image of the contact angle ( $91.29^\circ$ ) of the UV coating based on C8–303-polymer. (g) Image of the contact angle ( $108.06^\circ$ ) of the robust hydrophobic coating. (h) Image of the contact angle ( $102.77^\circ$ ) of the robust hydrophobic coating after being exposed outdoors for a month.

ABS, which was coated with the coating as shown in Figure 7b. The robust durable hydrophobic coating coated on the surface of PC and ABS underwent cross-cut and X-cut, then bonding and peeling by adhesive tape. The coating coated on PC and ABS had good adhesion of about level 0 or 1. Moreover, it still had adhesion of level 0 or 1 on surfaces such as PET and metal. As a contrast, the traditional UV coating based on PUA and EA has a poor adhesion of level 3 to 5, and it completely detached from the PET and metal surface.

Adhesion measured by cross-cut and X-cut shown in Figure 7b was followed ASTM D3359-17, the Standard Test Method for Rating Adhesion by Tape Test.

To test the anti-ink ability of a robust, durable hydrophobic coating, as shown in Figure 7c, the robust, durable hydrophobic coating and traditional UV coating based on PUA and EA resin were coated on the surface of glass and PCB, marked with a marking pen. The ink stain could be wiped off from the surface of the robust, durable hydrophobic coating but remained on the surface of the traditional UV coating based

on PUA and EA resin, which showed that the robust durable hydrophobic coating had a strong antigraffiti function. An experimental process video can be seen in the Supporting Information.

**3.5. Water Contact Angle of Robust, Durable Hydrophobic Coatings.** The contact angle is important in measuring hydrophobicity. We can see the contact angles of a series of UV coatings in Figure 8 and Figure 9. The contact angles of various traditional acrylic coatings range from  $40^\circ$  to  $70^\circ$  and generally do not exceed  $75^\circ$ . As illustrated by the contact angles of the three acrylic paints of formulas a, b, and c, hydrophobicity might relate to the cross-linking density. The cured film of UV coatings based on EP-POSS has contact angles of  $80^\circ$ – $90^\circ$ , for example,  $88.70^\circ$  for the UV coating based on 303-POSS. Groups such as long-chain alkyl or fluoroalkyl can enhance the hydrophobicity; for example, the contact angles of  $98.54^\circ$  and  $91.29^\circ$  were separately obtained by cured 3F-303-polymer and C8-303-polymer alone in our experiments.

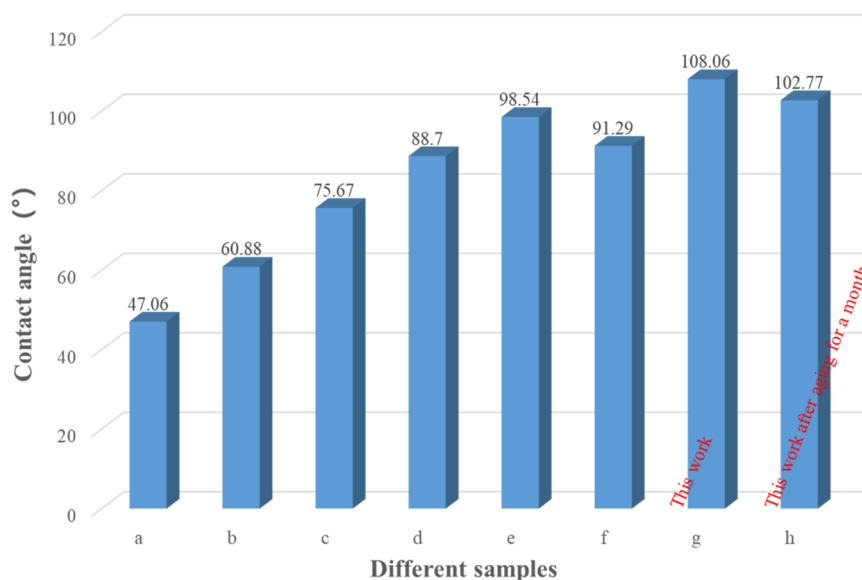


**Figure 9.** Statistics chart of different commercial coatings and the hydrophobic coating in this work.

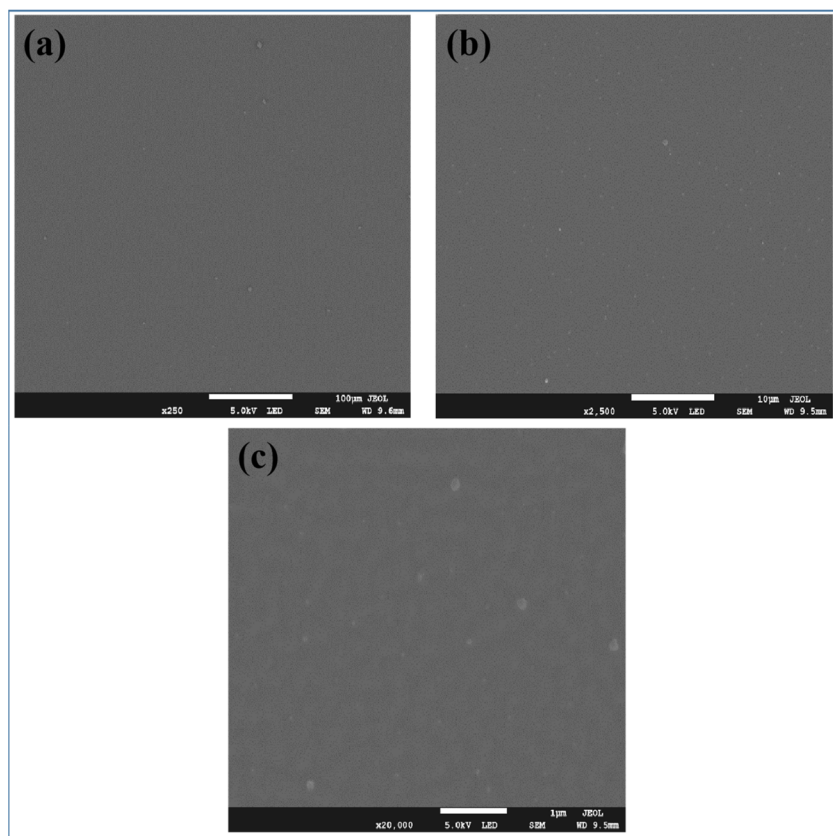


**Figure 10.** SEM images of robust hydrophobic coating. (a) SEM at magnification  $\times 150$  ( $100 \mu\text{m}$ ). (b) SEM at magnification  $\times 2500$  ( $10 \mu\text{m}$ ). (c) SEM at magnification  $\times 20\,000$  ( $1 \mu\text{m}$ ).

The dosage of 3F-402-polymer, 3F-303-polymer, C8-402-polymer, and C8-303-polymer should not exceed 10–20% for excessive dosage, leading to performance degradation, and the overall performance drops sharply while over 20–30%, manifesting longer times for curing, sticky surfaces, whitening of the cured film, and decreased hardness and adhesion.

Detailed experimental processes of formulas a, b, and c can be seen in the [Supporting Information S2](#).

**3.6. The Surface Morphology of Hydrophobic Coating.** To investigate what the hydrophobic characterization comes from, the morphology of hydrophobic coatings was analyzed by Scanning Electron Microscopy (SEM) and Atomic Force Microscopy (AFM). The results of SEM ( $100 \mu\text{m}$ ,  $10 \mu\text{m}$ ,  $1 \mu\text{m}$ ) are shown in [Figure 10](#), and the results of AFM are shown in [Figure 11](#).

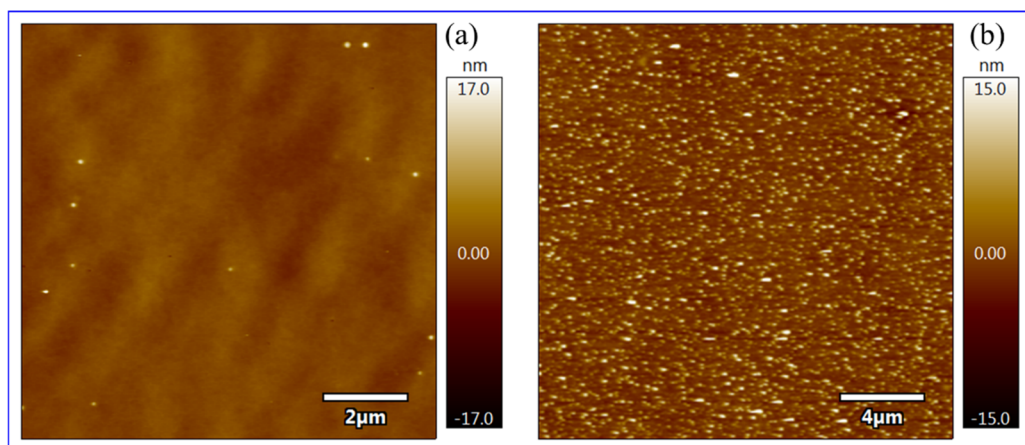


**Figure 11.** (a) AFM images of UV curable commercial coating based on PUA and EA. (b) AFM image of UV curable, robust, hydrophobic coating.

As shown in Figure 10, it is hard to demonstrate the microstructure even with a magnification of  $\times 20000$  ( $1 \mu\text{m}$ ) because it is almost impossible to distinguish the surface states. It seems that SEM is not a proper method, so we used AFM morphology scanning to study the surface roughness. As shown in Figure 11, in AFM images of a UV curable commercial coating based on PUA and EA (a) with  $R_q = 955.619 \text{ nm}$  and  $R_a = 725.289 \text{ nm}$  and an AFM image of a UV curable robust hydrophobic coating (b) with  $R_q = 2.708 \text{ nm}$  and  $R_a = 1.823 \text{ nm}$ , no hierarchical micro-nanostructure can be observed. Both roughness values of hydrophobic coating were higher than that of the commercial coating as reference samples. The  $R_a$  and  $R_q$  over the scanning range increased significantly and demonstrated the formation of an isolated island due to adding polymers containing hydrophobic groups (fluoroalkyl or long-chain alkyl) and nanoparticles. The results of SEM and AFM proved that the hydrophobicity of this UV curable, robust, hydrophobic coating depends on slight nanoscale roughness and low surface Gibbs free energy instead of hierarchical micro-nanostructure. The textured surface with slight nanoscale roughness could be easily obtained by a facile one-step approach, owing to the surface segregation of the fluoroalkyl polymer.

The formula of a UV curable commercial coating based on PUA and EA can be seen in formula b of Table S2 in the Supporting Information.

**3.7. Thermal Stability of the Series of Robust, Hydrophobic Coatings.** Considering that higher thermal stability can expand the practical application, TGA was employed to illustrate thermal stability. Compared with two samples of traditional UV coating based on PUA and EA and hydrophobic UV coating based on EP-POSS without inorganic fillers, the TGA test results were shown in Figure 12. The initial decomposition temperature of a traditional UV coating based on PUA and EA was around  $388 \text{ }^\circ\text{C}$ ; 16.7% remained at  $600 \text{ }^\circ\text{C}$ , and it completely carbonized at  $650 \text{ }^\circ\text{C}$  for the residue morphology after the test. But the data of the robust hydrophobic coating nearly reached  $427 \text{ }^\circ\text{C}$ , and 38.3% remained at  $600 \text{ }^\circ\text{C}$  and maintained a certain skeleton structure at  $650 \text{ }^\circ\text{C}$  for the residue morphology after the test.

The robust hydrophobic coatings were mainly composed of 303-POSS and their derivatives. The series of organic-inorganic intramolecular hybrid materials with a core-in-cage structure was constructed by repeating units  $\text{R-Si}(\text{O}_{1/2})_3$ , and the rigidity of the core-in-cage structure derived from the

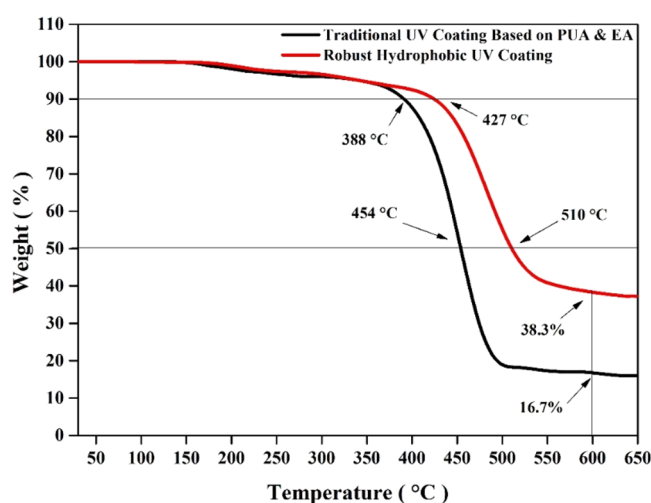


**Figure 12.** TGA of UV curable commercial coating and UV curable robust hydrophobic coating. TGA of the reference sample of a traditional UV coating based on PUA and EA without inorganic fillers (black) can be seen in formula b of Table S2 in the Supporting Information. TGA of mechanochemical robust hydrophobic durable coating without inorganic fillers is in red.

stability of the strong covalent bonds of Si–C and Si–O can highly improve the thermal performance of materials.

#### 4. CONCLUSIONS

The results showed that the series of EP-POSSs and their derivatives were successfully prepared through a sol-gel method. The structures of these polymers were determined by GPC, ATR-IR,  $^1\text{H}$  NMR, and Si NMR and other chemical tests. The results of  $^1\text{H}$  NMR and Si NMR showed that the products were not a compound with a single structure but a mixture of a series of similar substances. Performance test results showed that the pencil hardness of this UV curable robust hydrophobic coating was 6–8H; contact angles were  $108.06^\circ$  and changed to  $102.77^\circ$  after being exposed outdoors for a month. The surface morphology checked by SEM and AFM with a textured surface with slight nanoscale roughness proved that the hydrophobicity depended on slight nanoscale roughness and low surface Gibbs free energy instead of a hierarchical micro-nanostructure. Thermal analyses of TGA found that thermal stability was up to  $400 \text{ }^\circ\text{C}$ . Since this series of UV curable robust durable hydrophobic coatings based on

EP-POSSs and their derivatives exhibited so many excellent properties, it is conceivable that POSSs can show new ideas for the coating industry.

## ■ ASSOCIATED CONTENT

### SI Supporting Information

The Supporting Information is available free of charge at <https://pubs.acs.org/doi/10.1021/acsomega.2c00534>.

Supporting Video—wipe ink stains by dry tissue (MP4) All chemical materials used, seen in S1.1, Table S1; the synthesis process of the polymer described, seen in S1.2, S1.3, and S1.4; preparation of UV curable robust durable hydrophobic coating, seen in S1.5; the protocol of fabricating robust hydrophobic coating, seen in Scheme S1; characterization methods, seen in S1.6; the detailed experimental processes of formulas a, b, and c, seen in S1.7 (PDF)

## ■ AUTHOR INFORMATION

### Corresponding Authors

**Peng Zhang** – South China Advanced Institute for Soft Matter Science and Technology (AISMST), School of Emergent Soft Matter and Guangdong Provincial Key Laboratory of Functional and Intelligent Hybrid Materials and Devices, South China University of Technology, Guangzhou 510640, People's Republic of China; [orcid.org/0000-0002-2057-2108](https://orcid.org/0000-0002-2057-2108); Email: [841385430@139.com](mailto:841385430@139.com)

**Jianhui Xia** – South China Advanced Institute for Soft Matter Science and Technology (AISMST), School of Emergent Soft Matter and Guangdong Provincial Key Laboratory of Functional and Intelligent Hybrid Materials and Devices, South China University of Technology, Guangzhou 510640, People's Republic of China; [orcid.org/0000-0002-8857-3879](https://orcid.org/0000-0002-8857-3879); Email: [xiajh@scut.edu.cn](mailto:xiajh@scut.edu.cn)

### Author

**Ban Qin** – South China Advanced Institute for Soft Matter Science and Technology (AISMST), School of Emergent Soft Matter and Guangdong Provincial Key Laboratory of Functional and Intelligent Hybrid Materials and Devices, South China University of Technology, Guangzhou 510640, People's Republic of China

Complete contact information is available at:

<https://pubs.acs.org/doi/10.1021/acsomega.2c00534>

### Notes

The authors declare no competing financial interest.

## ■ ACKNOWLEDGMENTS

This work was supported by the Guangdong Provincial Key Laboratory of Functional and Intelligent Hybrid Materials and Devices (No. 2019B121203003), National Natural Science Foundation of China NSFC (No. 51890871), and The Recruitment Program of Guangdong (No. 2016ZT06C322).

## ■ REFERENCES

- (1) Zhu, Z.; Zheng, S.; Peng, S.; Zhao, Y.; Tian, Y. Superlyophilic Interfaces and Their Applications. *Adv. Mater.* **2017**, *29* (45), 1703120.
- (2) Ding, G.; Jiao, W.; Wang, R.; Niu, Y.; Hao, L.; Yang, F.; Liu, W. A biomimetic, multifunctional, superhydrophobic graphene film with self-sensing and fast recovery properties for microdroplet transportation. *J. Mater. Chem. A* **2017**, *5*, 17325.

- (3) Barthlott, W.; Neinhuis, C. Purity of the sacred lotus, or escape from contamination in biological surfaces. *PLANTA* **1997**, *202* (1), 1–8.
- (4) Zhang, X.; Shi, F.; Niu, J.; Jiang, Y.; Wang, Z. Superhydrophobic surfaces: from structural control to functional application. *J. Mater. Chem.* **2008**, *18*, 621.
- (5) Su, B.; Tian, Y.; Jiang, L. Bioinspired Interfaces with Superwettability: From Materials to Chemistry. *J. Am. Chem. Soc.* **2016**, *138* (6), 1727.
- (6) Nemani, S. K.; Annavarapu, R. K.; Mohammadian, B.; Raiyan, A.; Heil, J.; Haque, M. A.; Abdelaal, A.; Sojoudi, H. Surface Modification: Surface Modification of Polymers: Methods and Applications. *Adv. Mater. Interfaces* **2018**, *5* (24), 1870121.
- (7) Zhao, X.; Wei, C.; Gai, Z.; Yu, S.; Ren, X. Chemical vapor deposition and its application in surface modification of nanoparticles. *Chem. Pap.* **2020**, *74* (3), 767–778.
- (8) Nishimoto, S.; Bhushan, B. Bioinspired self-cleaning surfaces with superhydrophobicity, superoleophobicity, and superhydrophilicity. *RSC Adv.* **2013**, *3* (3), 671–690.
- (9) Liu, K.; Du, J.; Wu, J.; Jiang, L. Superhydrophobic gecko feet with high adhesive forces towards water and their bio-inspired materials. *Nanoscale* **2012**, *4*, 768.
- (10) Feng, X. J.; Jiang, L. Design and Creation of Superwetting/Antiwetting Surfaces. *Adv. Mater.* **2006**, *18* (23), 3063–3078.
- (11) Zheng, Y.; Gao, X.; Jiang, L. Directional adhesion of superhydrophobic butterfly wings. *Soft Matter* **2007**, *3*, 178.
- (12) Pan, S.; Guo, R.; Björnalm, M.; Richardson, J. J.; Li, L.; Peng, C.; Bertleff-Zieschang, N.; Xu, W.; Jiang, J.; Caruso, F. Coatings super-repellent to ultralow surface tension liquids. *Nat. Mater.* **2018**, *17* (11), 1040–1047.
- (13) Schutzius, T. M.; Jung, S.; Maitra, T.; Graeber, G.; Kohme, M.; Poulikakos, D. Spontaneous droplet trampolining on rigid superhydrophobic surfaces. *Nature* **2015**, *527* (7576), 82.
- (14) Schlaich, C.; Cuellar Camacho, L.; Yu, L.; Achazi, K.; Wei, Q.; Haag, R. Surface-Independent Hierarchical Coatings with Superamphiphobic Properties. *ACS Appl. Mater. Interfaces* **2016**, *8*, 29117.
- (15) Ge, M.; Cao, C.; Huang, J.; Li, S.; Chen, Z.; Zhang, K.-Q.; Al-Deyab, S. S.; Lai, Y. A review of one-dimensional TiO<sub>2</sub> nanostructured materials for environmental and energy applications. *J. Mater. Chem. A* **2016**, *4* (18), 6772–6801.
- (16) Kota, A. K.; Li, Y.; Mabry, J. M.; Tuteja, A. Hierarchically Structured Superoleophobic Surfaces with Ultralow Contact Angle Hysteresis. *Adv. Mater.* **2012**, *24*, 5838.
- (17) Rezaei, S.; Manoucheri, I.; Moradian, R.; Pourabbas, B. One-step chemical vapor deposition and modification of silica nanoparticles at the lowest possible temperature and superhydrophobic surface fabrication. *CHEM ENG J.* **2014**, *252*, 11.
- (18) Peng, S.; Yang, X.; Tian, D.; Deng, W. Chemically Stable and Mechanically Durable Superamphiphobic Aluminum Surface with a Micro/Nanoscale Binary Structure. *ACS Appl. Mater. Interfaces* **2014**, *6* (17), 15188.
- (19) Gao, L.; Gan, W.; Xiao, S.; Zhan, X.; Li, J. Enhancement of photo-catalytic degradation of formaldehyde through loading anatase TiO<sub>2</sub> and silver nanoparticle films on wood substrates. *RSC ADV* **2015**, *5*, 52985.
- (20) Zhao, H.; Law, K. Y. Super toner and ink repellent superoleophobic surface. *ACS Appl. Mater. Interfaces* **2012**, *4* (8), 4288–4295.
- (21) Ge, D.; Yang, L.; Wang, C.; Lee, E.; Zhang, Y.; Yang, S. A multi-functional oil–water separator from a selectively pre-wetted superamphiphobic paper. *Chem. Commun.* **2015**, *51* (28), 6149–52.
- (22) Darmanin, T.; Guittard, F. Molecular design of conductive polymers to modulate superoleophobic properties. *J. Am. Chem. Soc.* **2009**, *131* (22), 7928–7933.
- (23) Zhu, Q.; Chu, Y.; Wang, Z.; Chen, N.; Lin, L.; Liu, F.; Pan, Q. Robust superhydrophobic polyurethane sponge as a highly reusable oil-absorption material. *J. Mater. Chem. A* **2013**, *1* (17), 5386–5393.

- (24) Zhu, X.; Zhang, Z.; Men, X.; Yang, J.; Wang, K.; Xu, X.; Zhou, X.; Xue, Q. Robust superhydrophobic surfaces with mechanical durability and easy repairability. *J. Mater. Chem.* **2011**, *21* (39), 15793.
- (25) Li, Y.; Li, L.; Sun, J. Bioinspired Self-Healing Superhydrophobic Coatings. *Angew. Chem., Int. Ed. Engl.* **2010**, *122*, 6265.
- (26) Ahn, B. K.; Lee, D. W.; Israelachvili, J. N.; Waite, J. H. Surface-initiated self-healing of polymers in aqueous media. *Nat. Mater.* **2014**, *13* (9), 867–872.
- (27) Deng, X.; Mammen, L.; Butt, H.-J.; Vollmer, D. Candle Soot as a Template for a Transparent Robust Superamphiphobic Coating. *Science* **2012**, *335* (6064), 67–70.
- (28) Azimi, G.; Dhiman, R.; Kwon, H. M.; Paxson, A. T.; Varanasi, K. K. Hydrophobicity of rare-earth oxide ceramics. *Nat. Mater.* **2013**, *12* (4), 315–320.
- (29) Lu, Y.; Sathasivam, S.; Song, J.; Crick, C. R.; Carmalt, C. J.; Parkin, I. P. Robust self-cleaning surfaces that function when exposed to either air or oil. *Science* **2015**, *347* (6226), 1132–1135.
- (30) Peng, C.; Chen, Z.; Tiwari, M. K. All-organic superhydrophobic coatings with mechanochemical robustness and liquid impalement resistance. *Nat. Mater.* **2018**, *17* (4), 355–360.
- (31) Mishra, K.; Pandey, G.; Singh, R. P. Enhancing the mechanical properties of an epoxy resin using polyhedral oligomeric silsesquioxane (POSS) as nano-reinforcement. *Polym. Test.* **2017**, *62*, 210–218.
- (32) Yang, H.; He, C.; Russell, T. P.; Wang, D. Epoxy-polyhedral oligomeric silsesquioxanes (POSS) nanocomposite vitrimers with high strength, toughness, and efficient relaxation. *Giant* **2020**, *4*, 100035.
- (33) Scott, D. W. Thermal Rearrangement of Branched-Chain Methylpolysiloxanes. *J. Am. Chem. Soc.* **1946**, *68* (3), 356.
- (34) Brus, J.; Urbanova, M.; Strachota, A. Epoxy Networks Reinforced with Polyhedral Oligomeric Silsesquioxanes: Structure and Segmental Dynamics as Studied by Solid-State NMR. *Macromolecules* **2008**, *41* (2), 372–386.
- (35) Rashid, E.; Ariffin, K.; Kooi, C. C.; Akil, H. M. Preparation and properties of POSS/epoxy composites for electronic packaging applications. *Mater. Des.* **2009**, *30* (1), 1–8.
- (36) Sharma, A. K.; Sloan, R.; Wiggins, J. S. Epoxy hybrid networks with high mass fraction molecular-level dispersion of pendant polyhedral oligomeric silsesquioxane (POSS). *Polymer* **2017**, *114*, 298–310.
- (37) Fang, Y.; Wang, P.; Sun, L.; Wang, L. Hydrophobic Epoxy Caged Silsesquioxane Film (EP-POSS): Synthesis and Performance Characterization. *Nanomaterials* **2021**, *11* (2), 472.
- (38) Ikada, Y. Comparison of surface modification of polymers by different methods. *Radiat. Phys. Chem.* **1992**, *39* (6), 509–511.
- (39) Marquez, M.; Grady, B. P.; Robb, I. Different methods for surface modification of hydrophilic particulates with polymers. *Colloids Surf., A* **2005**, *266* (1–3), 18–31.
- (40) Goenner, E. S.; Creel, H. S.; Hine, A. M.; Kolb, B. U.; Portelli, G. B.; Thompson, W. L. Resin systems including reactive surface-modified nanoparticles. WO2008027979A2, 2009.
- (41) Brozek, E. M.; Zharov, I. Internal Functionalization and Surface Modification of Vinylsilsesquioxane Nanoparticles. *Chem. Mater.* **2009**, *21* (8), 1451.
- (42) Wang, X.; Wang, P.; Jiang, Y.; Su, Q.; Zheng, J. Facile surface modification of silica nanoparticles with a combination of noncovalent and covalent methods for composites application. *Compos. Sci. Technol.* **2014**, *104*, 1–8.
- (43) Choi, M.; Choi, W.-K.; Jung, C.-H.; Kim, S.-B. The surface modification and characterization of SiO<sub>2</sub> nanoparticles for higher foam stability. *Sci. Rep.* **2020**, *10* (1), 19399.
- (44) Nikolic, M. P.; Giannakopoulos, K. P.; Stamopoulos, D.; Moshopoulou, E. G.; Srdic, V. V. Synthesis and characterization of silica core/nano-ferrite shell particles. *Mater. Res. Bull.* **2012**, *47* (6), 1513–1519.
- (45) Baney, R. H.; Itoh, M.; Sakakibara, A.; Suzuki, T. Silsesquioxanes. *Chem. Rev.* **1995**, *95* (5), 1409–1430.